Asymmetric Collaborative Bar Stabilization Tethered to Two Heterogeneous Aerial Vehicles

Pedro O. Pereira and Pedro Roque and Dimos V. Dimarogonas

Abstract

We consider a system composed of a bar tethered to two unmanned aerial vehicles (UAVs), where the cables behave as rigid links under tensile forces, and with the control objective of stabilizing the bar's pose around a desired pose. Each UAV is equipped with a PID control law, and we verify that the bar's motion is decomposable into three decoupled motions, namely a longitudinal, a lateral and a vertical. We then provide relations between the UAVs' gains, which, if satisfied, allows us to decompose each of those motions into two cascaded motions; the latter relations between the UAVs' gains are found so as to counteract the system asymmetries, such as the different cable lengths and the different UAVs' weights. Finally, we provide conditions, based on the system's physical parameters, that describe *good* and *bad* types of asymmetries. We present experiments that demonstrate the stabilization of the bar's pose.

I. Introduction

Aerial vehicles provide a platform for transportation of cargos in dangerous and cluttered environments [1]. In particular, vertical take off and landing rotorcrafts, with hovering capabilities, have been used to validate different types of transportation and manipulation of objects.

Tethered transportation, when compared with transportation by manipulators, is mechanically simple and inexpensive. Several control strategies for slung-load transportation, i.e., tethered transportation of a point mass load by a single UAV, are found in the literature. The swing angle of the load can be estimated, either inferred from vision or from the internal force exerted by the load on the UAV, and used in the feedback loop to avoid/dampen swing excitation [2]–[4]. Trajectory planning that minimizes the loads' swing, and exploiting differential flatness for control purposes has also been demonstrated [5]–[7].

Cooperative transportation with multiple UAVs is also found in the literature. Vision has been used to correctly place end-effectors with respect to a visual target placed on the object to be transported [8]–[10], or to autonomously estimate the bar's pose [11]. Motion planning for collision avoidance between the cargo and the UAVs with obstacles in a cluttered environment has also been studied and validated [12]–[15]. How to position a group UAVs by specifying the desired tension on the cables and a desired pose for the tethered object is found in [16], [17]. Note that tethered transportation with multiple UAVs comes with multiple degrees of freedom, which have been explored so as to minimize the internal forces applied of the load [18], [19]. Different approaches are found regarding the grasping mechanism in aerial transportation, such as, adhesive/gripping mechanisms at the tool-tip that stick to the grasped object [20]; a hook-based system between the end-effector and the point to grasp [15]; and magnets, electromagnets and electropermanent magnets [21] – the latter is the option we adopt.

In this manuscript, we focus on stabilization of a rod-like object tethered to two AUVs, as pictured in Fig. 1. This problem has also been considered in [11], [22], [23]. In [22], a master-slave approach for the two UAVs is put in place, with the slave UAV estimating the cable force exerted on itself. In [11], vision is used to autonomously estimate the bar's pose. In [23], relations on the UAVs' PID gains are provided for which stability – regarding the bar's pose stabilization – is guaranteed.

Regarding experimental cooperative transportation, experiments have been performed where the system is taken to be symmetric [11], [11], [15], [22], [23]. In this work, we extend [23], and consider an asymmetric system, with non-identical UAVs and different cable lengths. We perform an analysis similar to that in [3], [24], [25], where we linearize the system, and derive conditions on the gains that guarantee exponential stability regarding the stabilization of the bar's pose. We verify that the bar's motion is decomposable into three decoupled motions, namely a longitudinal, a lateral and a vertical; and that if UAVs' gains satisfy specific relations, each of those motions is in turn decomposable into two cascaded motions: f.e., the vertical motion is decomposable into the vertical linear motion and the vertical angular motion of the bar, with the latter cascaded after the former, if the vertical PID gains of the two UAVs satisfy a specific ratio (which is unitary if the system is symmetric). We also show that the bar behaves similarly to container in a container-crane system [26], i.e., the bar's longitudinal and lateral motion can be compared to that of container. Finally, we provide conditions, based on the system's physical parameters, that describe *good* and *bad* types of asymmetries: f.e., it is better for the heavier vehicle to be attached to the shorter cable, in the sense that stability is guaranteed by a smaller proportional gain. These conditions can be explored to design safer experiments.

The remainder of this paper is structured as follows. In Sections III and IV, the model of the system and the contol law are described. In Section V, we present conditions under which matrices of interest are Hurwitz; and we also briefly describe

The authors are with the School of Electrical Engineering, KTH Royal Institute of Technology, SE-100 44, Stockholm, Sweden. {ppereira, dimos}@kth.se. This work was supported by the EU H2020 Research and Innovation Programme under GA No.644128 (AEROWORKS), the Swedish Research Council (VR), the Swedish Foundation for Strategic Research (SSF) and the KAW Foundation.

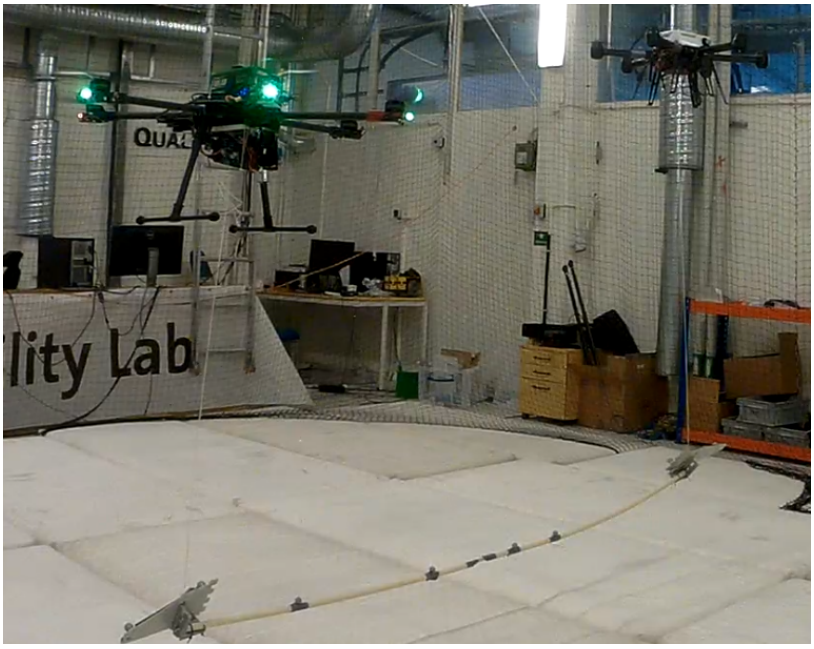

Fig. 1: Tethered transportation of a rod-like object by two heterogeneous aerial vehicles, with different cable lengths.

the container-crane dynamics, which we then compare with the UAVs-bar dynamics. In Section VI, we linearize the closed loop vector field around the equilibrium and, under a proper similarity matrix and a proper choice of gains, we verify the longitudinal, lateral and vertical motion decomposition. Finally, in Section VII, we present illustrative experimental results.

This document is to be read in conjunction with the mathematica notebook files available in the repository.

II. Notation

The map $\mathcal{S}:\mathbb{R}^3\ni x\mapsto\mathcal{S}(x)\in\mathbb{R}^{3\times3}$ yields a skew-symmetric matrix and it satisfies $\mathcal{S}(a)\,b=a\times b$, for any $a,b\in\mathbb{R}^3$. $\mathbb{S}^2:=\{x\in\mathbb{R}^3:x^Tx=1\}$ denotes the set of unit vectors in $\mathbb{R}^3$. We denote $A_1\oplus\cdots\oplus A_n$ as the block diagonal matrix with block diagonal entries A_1 to A_n (square matrices). We denote by $e_1,\cdots,e_n\in\mathbb{R}^n$ the canonical basis vectors in $\mathbb{R}^n$, for some $n\in\mathbb{N}$. Given some $n,m\in\mathbb{N}$, and a function $f:\mathbb{R}^n\ni a\mapsto f(a)\in\mathbb{R}^m$, $f':\mathbb{R}^n\ni a\mapsto f'(a)\in\mathbb{R}^{m\times n}$ denotes the derivative of f.

III. Problem Description

Consider the system illustrated in Fig. 2, with two VTOL aerial vehicles, a one dimensional bar and two cables connecting the aerial vehicles to distinct contact points on the bar. Fig. 2 provides a two-dimensional picture of the real system, as shown in Fig 1, but the modeling we describe next is three dimensional. Hereafter, and for brevity, we refer to this system as UAVs-bar system. We denote by $p_1,p_2,p\in\mathbb{R}^3$ and by $v_1,v_2,v\in\mathbb{R}^3$ the UAVs' and the bar's center of mass positions and velocities; by $n,\omega\in\mathbb{R}^3$ the bar's orientation and angular velocity; by $r_1,r_2\in\mathbb{S}^2$ the UAV's thrust directions; and by $\xi_1,\xi_2\in\mathbb{R}$ the vertical integral error of each UAV. As for physical constants, we denote by $m_1,m_2,m>0$ the UAVs' and bar's masses; by $J>0$ the bar's moment of inertia (w.r.t. the bar's center of mass); by $l_1,l_2>0$ the cables' lengths; and, finally, by $d_1,d_2\in\mathbb{R}$ the contact points on the bar at which the cables are attached to. Finally, we denote by $u_1,u_2\in\mathbb{R}^3$ the input forces on the UAVs-bar system: for $i\in\{1,2\}$, $\bar{u}_i:=U_ir_i:=u_i^Tr_ir_i$ is the UAV i input force, where the throttle U_i is taken as the inner product between the input u_i and the UAVs thrust direction (one may think of u_i as the desired value for $\bar{u}_i$).

For brevity, given the quantities described above, denote

$$z:=(p,n,p_1,p_2,v,\omega,v_1,v_2,r_1,r_2,\xi_1,\xi_2)\in\mathbb{R}^{32} \tag{1}$$

$$u:=(u_1,u_2)\in\mathbb{R}^6 \tag{2}$$

where z in (1) is used next as the state of the UAVs-bar system, and u in (2) is used next as the input of the UAVs-bar

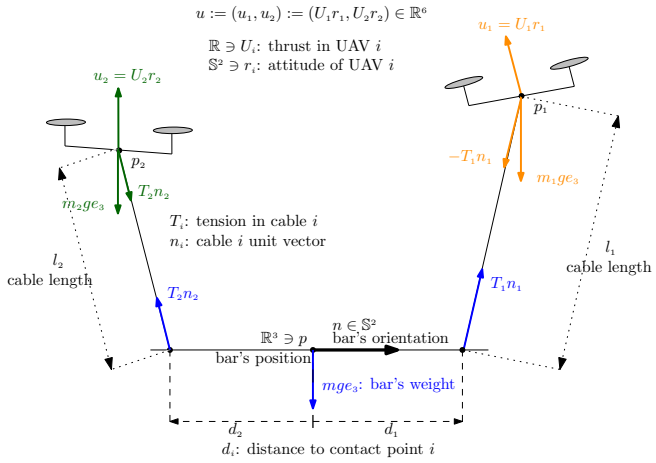

Fig. 2: Modeling of UAVs-bar system

system. Consider then the state space

$$\mathbb{Z} := \{z \in \mathbb{R}^{32} : f(z) = 0_8\}, \tag{3}$$

$$f(z) := \begin{bmatrix} n^T n - 1 \\ n^T \omega \\ \|p + d_1 n - p_1\|^2 - l_1^2 \\ \|p + d_2 n - p_2\|^2 - l_2^2 \\ (p + d_1 n - p_1)^T (v + d_1 \mathcal{S}(\omega) n - v_1) \\ (p + d_2 n - p_2)^T (v + d_2 \mathcal{S}(\omega) n - v_2) \\ r_1^T r_1 - 1 \\ r_2^T r_2 - 1 \end{bmatrix} \tag{4}$$

where the map $f : \mathbb{R}^{32} \ni z \to f(z) \in \mathbb{R}^8$ defined above encapsulates the constraints illustrated in Fig. 2. Specifically, the first two constraints in (4) imply that the bar's attitude n is given by a unit vector and the bar's angular velocity ω is orthogonal to that unit vector (rotations around the bar itself do not affect the bar's attitude); the next four constraints in (4), imply that the distance between each contact point on the bar and the corresponding UAV is constant and equal to the corresponding cable length; and, finally, the last two constraints in (4), imply that the UAVs' thrust vectors are also given by a unit vectors.

Given an appropriate input $u : \mathbb{R}_{\geq 0} \mapsto \mathbb{R}^6$, a system's trajectory $z : \mathbb{R}_{\geq 0} \ni t \mapsto z(t) \in \mathbb{Z}$ evolves according to

$$\dot{z}(t) = Z(z(t), u(t)), z(0) \in \mathbb{Z}, \tag{5}$$

where the vector field $Z : \mathbb{Z} \times \mathbb{R}^6 \ni (z, u) \mapsto Z(z, u) \in \mathbb{R}^{32}$ is given by

$$Z(z, u) := \begin{bmatrix} Z_k(z) \\ Z_d(z, u) \\ Z_r(z, u) \\ Z_i(z) \end{bmatrix} \left(= \begin{bmatrix} \text{kinematics} \\ \text{dynamics} \\ \text{attitude inner loop} \\ \text{integrator dynamics} \end{bmatrix} \right), \tag{6}$$

with the kinematics given by

$$Z_k(z) := (v, \mathcal{S}(\omega) n, v_1, v_2) \, (= (\dot{p}, \dot{n}, \dot{p}_1, \dot{p}_2)),$$

with the dynamics given by (below, g stands for the acceleration due to gravity; T_1, T_2 stand for the tensions on the cables, which are functions of the state and the input; and $n_i \equiv \frac{p_i - (p + d_i n)}{l_i}$ stands for the cable $i \in \{1, 2\}$ direction)

$$Z(z, u) := \begin{bmatrix} \sum_{i \in \{1,2\}} \frac{T_i(z, \bar{u})}{m} n_i - g e_3 \\ \sum_{i \in \{1,2\}} \frac{T_i(z, \bar{u})}{J} \mathcal{S}(d_i n) n_i \\ \frac{\bar{u}_1}{m_1} - \frac{T_1(z, \bar{u})}{m_1} n_1 - g e_3 \\ \frac{\bar{u}_2}{m_2} - \frac{T_2(z, \bar{u})}{m_2} n_2 - g e_3 \end{bmatrix} \left(= \begin{bmatrix} \dot{v} \\ \dot{\omega} \\ \dot{v}_1 \\ \dot{v}_2 \end{bmatrix} \right),$$

$$\bar{u} \equiv (\bar{u}_1, \bar{u}_2) \equiv (u_1^T r_1 r_1, u_2^T r_2 r_2)$$

with the attitude inner loop dynamics given by (below, k_r^1, k_r^2 stand for the positive gains of the attitude inner loop of the

vehicles)

$$Z_r(z,u) := \begin{bmatrix} \mathcal{S}\left(k_r^1 \mathcal{S}\left(r_1\right) \frac{u_1}{\|u_1\|}\right) r_1 \\ \mathcal{S}\left(k_r^2 \mathcal{S}\left(r_2\right) \frac{u_2}{\|u_2\|}\right) r_2 \end{bmatrix} \left(= \begin{bmatrix} \dot{r}_1 \\ \dot{r}_2 \end{bmatrix} \right), \tag{7}$$

and, finally, with the integrator dynamics given by

$$Z_i(z,u) := \begin{bmatrix} e_3^T p_1 - l_1 \\ e_3^T p_2 - l_2 \end{bmatrix} \left(= \begin{bmatrix} \dot{\xi}_1 \\ \dot{\xi}_2 \end{bmatrix} \right). \tag{8}$$

An important relation to note is that

$$\underbrace{f'(z)}_{\mathbb{R}^{8\times 32}} \underbrace{Z(z,u)}_{\mathbb{R}^{32}} = 0_8, \text{ for all } (z,u) \in \mathbb{Z} \times \mathbb{R}^6, \tag{9}$$

which simply implies that a solution of (5) starting in $\mathbb{Z}$, remains in $\mathbb{Z}$ (i.e., that $\mathbb{Z}$ is invariant).

Let us provide some details on the vector field 6. The dynamics equations are be obtained from the Newton-Euler's equations of motion, considering the net force and torque on each rigid body: the bar is taken as a rigid body (with net force and torque in blue – see Fig. 2); while the UAVs are taken as point masses (with net forces in orange and green – see Fig. 2). The Newton-Euler's equations of motion do not provide any insight into the tensions T_1 and T_2 since these constitute internal forces: the tensions are found by guaranteeing the dynamics are within the state space tangent set. This constraint uniquely defines the tensions on the cable, i.e., for any $(z,u) \in \mathbb{Z} \times \mathbb{R}^6$, $Z(z,u) \in T_z\mathbb{Z}$ implies that

$$\begin{bmatrix} T_1(z,u) \\ T_2(z,u) \end{bmatrix} = \tilde{M}_T^{-1}(z_k) \left(\begin{bmatrix} \frac{m}{m_1} n_1(z_k)^T & 0_{1\times 3} \\ 0_{1\times 3} & \frac{m}{m_2} n_2(z_k)^T \end{bmatrix} \begin{bmatrix} u_1 \\ u_2 \end{bmatrix} + m \begin{bmatrix} \frac{\|v_1 - (v + d_1 \mathcal{S}(\omega) n)\|^2}{l_1} \\ \frac{\|v_2 - (v + d_2 \mathcal{S}(\omega) n)\|^2}{l_2} \end{bmatrix} + m\|\omega\|^2 \begin{bmatrix} d_1 n^T n_1(z_k) \\ d_2 n^T n_2(z_k) \end{bmatrix} \right), \text{ where}$$

$$\tilde{M}_T(z_k) = \begin{bmatrix} \frac{m}{m_1} & 0 \\ 0 & \frac{m}{m_2} \end{bmatrix} + \begin{bmatrix} 1 & \cos(\theta) \\ \cos(\theta) & 1 \end{bmatrix} + \frac{m d_1 d_2}{J} \begin{bmatrix} \frac{d_1}{d_2}\|a\|^2 & a^T b \\ a^T b & \frac{d_2}{d_1}\|b\|^2 \end{bmatrix} \Big|_{\substack{\cos(\theta) = n_1(z_k)^T n_2(z_k) \\ a = \mathcal{S}(n) n_1(z_k) \\ b = \mathcal{S}(n) n_2(z_k)}}.$$

The attitude inner loop dynamics in (7) is a simple first order model with attitude gain $k_r > 0$, that guarantees that the UAV $i \in \{1,2\}$ thrust vector tries to align itself with the direction of the input force u_i (for a constant $u_i \in \mathbb{R}^3 \backslash \{0_3\}$, a solution of $\dot{r}_i = k_r \mathcal{S}\left(r_i\right) \mathcal{S}\left(r_i\right) \frac{u_i}{\|u_i\|}$ converges exponentially fast to $\frac{u_i}{\|u_i\|}$, with rate proportional to k_r). Note that the model for the attitude inner loop of the UAVs in (7) is only a possible one, and there are more ways of modeling that inner loop.

Let us define the equilibrium, before explaining the integrator dynamics in (8). For any $\xi^\star := (\xi_1^\star, \xi_2^\star) \in \mathbb{R}^2$, define

$$\begin{aligned} z^\star &:= (p^\star, n^\star, p_1^\star, p_2^\star, v^\star, \omega^\star, v_1^\star, v_2^\star, r_1^\star, r_2^\star, \xi_1^\star, \xi_2^\star) \in \mathbb{Z} \\ &:= (0_3, e_1, d_1 e_1 + l_1 e_3, d_2 e_1 + l_2 e_3, 0_3, 0_3, 0_3, 0_3, e_1, e_1, \xi_1^\star, \xi_2^\star), \end{aligned} \tag{10}$$

and $u^\star := (u_1^\star, u_2^\star) \in \mathbb{R}^6$ as

$$u^\star := \left(\left(m_1 + \frac{m d_2}{d_2 - d_1} \right) g e_3, \left(m_2 + \frac{m d_1}{d_1 - d_2} \right) g e_3 \right). \tag{11}$$

Since $Z(z^\star, u^\star) = 0_{32}$, it follows that $z^\star$ (under a constant input $u^\star$) is an equilibrium of the system. As such, the integral terms (ξ_1 and ξ_2) evolving according to the integrator dynamics in (8) represent the z-position integral error of the UAVs. These integral errors are used in the control law, and provide robustness again disturbances and model uncertainties, as shall be verified in the experiments.

We can now formulate the problem treated in this paper.

Problem 1: Given the vector field Z in (6) and the equilibrium $z^\star$ in (10) (for some $(\xi_1^\star, \xi_2^\star) \in \mathbb{R}^2$), design a control law $u^{cl} : \mathbb{Z} \mapsto \mathbb{R}^6$ satisfying $u^{cl}(z^\star) = u^\star$ and such that $z^\star$ is an exponentially stable equilibrium of the closed loop vector field $z \mapsto Z(z, u^{cl}(z))$.

Remark 1: In general, we may require the bar to stabilize around any point $p^\star \in \mathbb{R}^3$ and any attitude $n^\star \in \mathbb{S}^2$ with $e_3^T n^\star = 0$. For that purpose, if suffices to place the origin of the inertial frame at $p^\star$, and align the inertial x-axis with $n^\star$: i.e., stabilizing around the pose $(p^\star, n^\star)$ is reduced to stabilizing around the pose $(0_3, e_1)$ as indicated in the equilibrium (10).

IV. Control Law

For each aerial vehicle – $i \in \{1,2\}$ – consider the PID-like control law $u_i^{pid} : \mathbb{Z} \ni z \mapsto u_i^{pid}(z) \in \mathbb{R}^3$ defined as

$$u_i^{pid}(z) := (u_{i,x}^{pd}(z), u_{i,y}^{pd}(z), u_{i,z}^{pid}(z)), \tag{12}$$

where

$$\begin{aligned} u^{pd}_{i,x}(z) &:= -m_i(k^i_{p,x}e_1^T(p_i - p_i^\star) + k^i_{d,x}e_1^T v_i) \\ u^{pd}_{i,y}(z) &:= -m_i(k^i_{p,y}e_2^T(p_i - p_i^\star) + k^i_{d,y}e_2^T v_i) - m_i d_i l_i \left(k^i_{p,\psi}e_2^T n + k^i_{d,\psi}e_3^T\omega\right) \\ u^{pid}_{i,z}(z) &:= -m_i(k^i_{p,z}e_3^T(p_i - p_i^\star) + k^i_{d,z}e_3^T v_i + k^i_{i,z}\xi_i) \end{aligned} \tag{13}$$

where $p_1^\star, p_2^\star$ are the UAVs equilibrium positions given in (10); where $k^i_{p,j}$ and $k^i_{d,j}$, for $j \in \{x, y, z\}$, are positive gains related to the position and velocity feedback, respectively, of vehicle $i \in \{1, 2\}$; and where $k^i_{i,z}$ is a positive gain related to the integral feedback of vehicle $i \in \{1, 2\}$.

Remark 2: The real control law is subject to saturations, which are of practical importance. To be specific, for the saturation function

$$\mathbb{R} \times \mathbb{R}_{>0} \ni (x, \sigma) \mapsto \sigma(x, \sigma) := \frac{\sigma x}{\sqrt{\sigma^2 + x^2}} \in (-\sigma, \sigma),$$

the real control law in (12) is of the form

$$\begin{aligned} u^{pd}_{i,x}(z) &:= -m_i(k^i_{p,x}\sigma(e_1^T(p_i - p_i^\star), \sigma_{p,x}) + k^i_{d,x}\sigma(e_1^T v_i, \sigma_{d,x})) \\ u^{pd}_{i,y}(z) &:= -m_i(k^i_{p,y}\sigma(e_2^T(p_i - p_i^\star), \sigma_{p,y}) + k^i_{d,y}\sigma(e_2^T v_i, \sigma_{d,y})) - m_i d_i l_i \left(k^i_{p,\psi}e_2^T n + k^i_{d,\psi}\sigma(e_3^T\omega, \sigma_{\omega,y})\right), \\ u^{pid}_{i,z}(z) &:= -m_i(k^i_{p,z}\sigma(e_3^T(p_i - p_i^\star), \sigma_{p,z}) + k^i_{d,z}\sigma(e_3^T v_i, \sigma_{d,z}) + k^i_{i,z}\sigma(\xi_i, \sigma_{i,z})), \end{aligned} \tag{14}$$

for some positive saturations $\sigma_{p,x}, \sigma_{d,x}, \sigma_{p,y}, \sigma_{d,y}, \sigma_{\omega,y}, \sigma_{p,z}, \sigma_{d,z}$. Note however that linearizing (14) around $z^\star$ in (10) yields (13). As such, since the saturations do not play a role when linearizing around the equilibrium point, we may ignore them for the rest of this manuscript.

Let us provide some insight into the control law (12) (and recall that we wish to align the bar with the inertial x direction, i.e., $n^\star = e_1$). The control law along the x-direction ($u^{pd}_{i,x}$) is composed of two terms, one proportional and one derivative that try to bring the UAV to its desired x position: this control law will only influence the x linear motion of the bar, and the motion x linear motion between the UAVs. The control law along the y-direction ($u^{pd}_{i,y}$) is composed of four terms: one proportional and one derivative that try to bring the UAV to its desired y position; and one proportional and one derivative that try to bring the bar to its desired y angular position: this control law will only influence the y linear motion of the bar, as well as the y angular motion of the bar (the yaw motion). Finally, the control law along the z-direction ($u^{pid}_{i,z}$) is composed of three terms: a proportional, a derivative and an integral that try to bring the UAV to its desired z position. this control law will only influence the z linear motion of the bar, as well as the z angular motion of the bar (the pitch motion).

Given the equilibrium input defined in (11), the complete control law is then defined as

$$\mathbb{Z} \ni z \mapsto u^{cl}(z) := u^\star|_{m=\hat{m}} + (u_1^{pid}(z), u_2^{pid}(z)) \in \mathbb{R}^6,$$

where $\hat{m}$ is the expected mass of the bar: f.e., if the the bar's weight is known, then $\hat{m} := m$, if the bar's weight is unknown, then $\hat{m} := 0$. It then follows that for (see Problem 1 and (11))

$$(\xi_1^\star, \xi_2^\star) := \left(\frac{g}{k^1_{i,z}}\frac{(m - \hat{m})d_2}{m_1(d_2 - d_1)}, \frac{g}{k^2_{i,z}}\frac{(m - \hat{m})d_1}{m_2(d_1 - d_2)}\right) \Rightarrow u^{cl}(z^\star) = u^\star, \tag{15}$$

where we emphasize that if the bar's weight is known, then the equilibrium integral errors vanish, i.e., $(\xi_1^\star, \xi_2^\star) = (0, 0)$; however, even if the bar's weight is know, having integral errors is still a good practical solution as it provides robustness against other model uncertainties. In the next Sections, we study the stability of the equilibrium $z^\star$ (with $(\xi_1^\star, \xi_2^\star)$ as in (15)) of the closed loop vector field

$$z \mapsto Z^{cl}(z) := Z(z, u^{cl}(z)) \tag{16}$$

V. Routh's Criterion

In Section **??**, we linearize the closed loop vector field around the equilibrium, and we verify that the Jacobian is similar to a block triangular matrix, whose block diagonal entries are in controllable form. This section provides immediate tools for the analysis of the eigenvalues of those matrices in controllable form. Denote then, for any $n \in \mathbb{N}$,

$$C_n(a) := \begin{bmatrix} 0 & 1 & 0 & \cdots & 0 \\ 0 & 0 & 1 & \cdots & 0 \\ \vdots & \vdots & \vdots & \ddots & \vdots \\ 0 & 0 & 0 & \cdots & 1 \\ -a_0 & -a_1 & -a_2 & \cdots & -a_{n-1} \end{bmatrix},$$

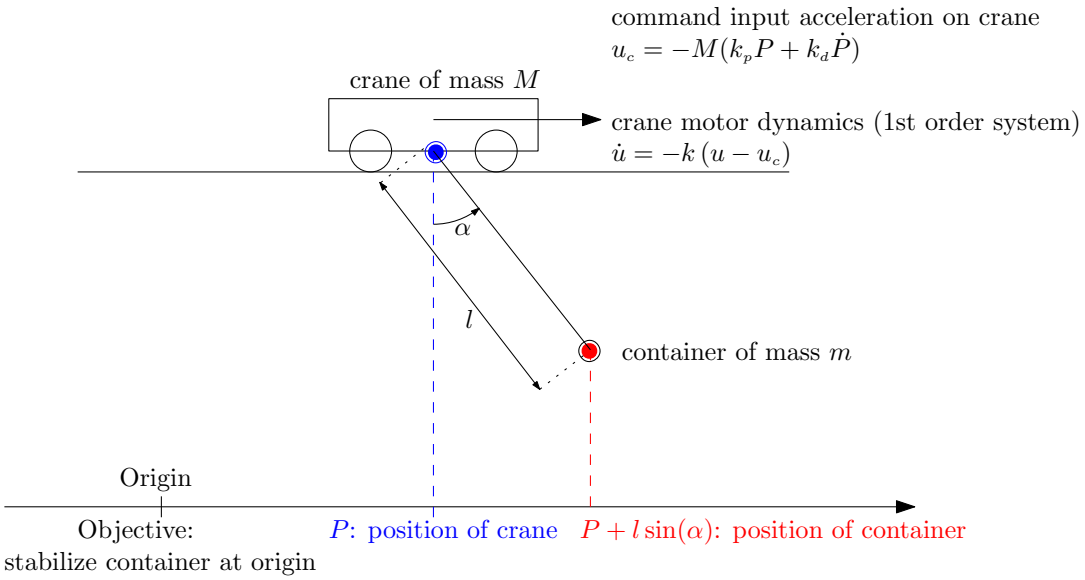

Fig. 3: Container crane system, where crane motor has the dynamics of a first order system. Tethered transportation of a bar can decomposed in three motions that have similar dynamics to those of a container crane

as a matrix in controllable form, and whose eigenvalues are those in $\{\lambda \in \mathbb{C} : \sum_{i=0}^{i=n} a_i \lambda^i = 0\}$. It follows from the Routh's criterion that

$$C_3((a_0, a_1, a_2)) \text{ Hurwitz} \Leftrightarrow a_0, a_1, a_2 > 0 \wedge a_0 < a_1 a_2, \tag{17}$$

which we make use of later on. In what follows, denote $p := (p_1, p_2) \in \mathbb{R}^2$, $f := (f_p, f_d) \in (\mathbb{R}_{\geq 0})^2$, $k := (k_p, k_d) \in (\mathbb{R}_{\geq 0})^2$, where, in later sections, p and f provide physical constants of interest, and k provides the controller gains (in particular a proportional and a derivative gain). There are two matrices (in controllable form) that appear several times in Section VI, and therefore we introduce them here. Specifically, we define Γ_3 and Γ_4 as

$$\Gamma_3(f, k) := C_3((f_d(k_p + f_p), f_d k_d + f_p, f_d)), \tag{18}$$

$$\Gamma_5(p, f, k) := C_5(b_1 + b_2)|_{\substack{b_1 \equiv (f_d f_p (k_p + f_p p_1), f_p (f_d k_d + f_p p_1), f_d k_p, f_d k_d, f_d), \\ b_2 \equiv f_p (1 + p_2 + p_1)(0, 0, f_d, 1, 0)}}, \tag{19}$$

Since we are interested in determining the stability of an equilibrium, it proves useful to determine when a matrix is Hurwitz. That it is the case iff all the elements in the first column of the Routh's table are positive (or negative) [27], and you can find these columns in the mathematica files. It follows from the Routh's criterion that (18) and (19) are Hurwitz if and only if

$$p_2 > 0, f_d > \frac{k_p}{k_d}, \text{ and } k_p > \max(0, -f_p p_1). \tag{20}$$

Remark 3: Note from (**??**) that p_1 is a parameter that perturbs the proportional and the derivative gains, and (20) simply implies that the perturbed gains in (**??**) need to be positive.

A. Crane system

As we will verify in the next Section, the tethered transportation of a bar can decomposed in three motions that have similar dynamics to those of a container crane. Let us then give some intuition for the results that follow by considering the container-crane system, as illustrated in Fig. 3, where the goal is to stabilize the position of the container at the origin. The dynamics of this system can be found in the mathematica notebook "crane_system/crane_system.nb", which are derived by means of the Lagrangian formalism. Under the control law shown in Fig. 3, one obtains a closed loop state matrix

$$A := \begin{bmatrix} 0 & 0 & 1 & 0 & 0 \\ 0 & 0 & 0 & 1 & 0 \\ 0 & g\frac{m}{M} & 0 & 0 & \frac{1}{M} \\ 0 & -\frac{g}{l}\frac{m+M}{M} & 0 & 0 & -\frac{1}{lM} \\ -kk_pM & 0 & -kk_dM & 0 & -k \end{bmatrix} \in \mathbb{R}^{5\times 5}.$$

However, A is not in a form that allows for easily checking the location of its eigenvalues (their location w.r.t. to the imaginary axis, to be more precise). This motivates the introduction of a similarity transformation, namely

$$P := \begin{bmatrix} p & Ap & A^2p & A^3p & A^4p \end{bmatrix} \in \mathbb{R}^{5\times 5}, \tag{21}$$

$$p := e_1 + le_2 \in \mathbb{R}^5, \tag{22}$$

It then follows that (recall Γ_5 in (19))

$$\bar{A} = PAP^{-1} = \Gamma_5\left((p_1, p_2), (f_p, f_d), (k_p, k_v)\right)$$

where

$$f_p = \frac{g}{l}, f_d = k, p_1 = 0, p_2 = \frac{m}{M}.$$

Notice that f is the (squared) frequency of the pendulum. If follows from (20), that if

$$k > \frac{k_p}{k_d} \Leftrightarrow \text{motor gain} > \frac{\text{proportional gain}}{\text{derivative gain}},$$

then PAP^{-1}, and therefore A, is Hurwitz. In other words, if the motor is *fast enough* (the precise meaning is encoded in the inequality above), the container is stabilized around the origin, under the control law shown in Fig 3. One can also provide an interpretation for the similarity matrix P in (21): it implies that, for the linearized motion, the position of the container, i.e., p as defined in (22), behaves as a fifth order integrator, i.e.,

$$p^{(5)}(t) = \bar{A}_{5,1}p^{(0)}(t) + \cdots + \bar{A}_{5,5}p^{(4)}(t). \tag{23}$$

Studying the stability of this motion is equivalent to studying the location of the roots of the characteristic polynomial, i.e., $\{s \in \mathbb{C} : s^5 = \bar{A}_{5,1}s^0 + \cdots + \bar{A}_{5,5}s^4\}$, which justifies the results presented in Section V.

VI. Linearization

Before linearizing the closed loop vector field Z^{cl} in (16) around the equilibrium $z^\star$ in (10), let us provide a vector field that serves only the purpose of analysis. Recall the map f in (4), representing the constraints on the state space. Consider then, for any $z \in \mathbb{R}^{32}$ and for some $\lambda > 0$,

$$\tilde{Z}(z) = -f'(z^\star)^T\left(f'(z^\star)f'(z^\star)^T\right)^{-1}\left(f'(z)Z^{cl}(z) + \lambda f(z)\right), \tag{24}$$

where, it follows from (3) and (9), that for any $z \in \mathbb{Z}$, $\tilde{Z}(z) = 0_{32}$ (the inverse above is well defined, since the determinant of the matrix being inverted is positive: $|f'(z^\star)f'(z^\star)^T| = (2^5(3(1-2d_1d_2)+2(d_1+d_2)^2))^2 > 0$). Consider then the new vector field

$$\bar{Z}^{cl}(z) := Z^{cl}(z) + \tilde{Z}(z) \tag{25}$$

where we emphasize that $\bar{Z}^{cl}(z) = Z^{cl}(z)$ for any $z \in \mathbb{Z}$. The sole purpose of the vector field $\tilde{Z}$ is to permit the analysis we do next.

Linearization of the closed loop vector field $\bar{Z}^{cl}$ in (25) around $z^\star$ in (10) yields the Jacobian

$$A := D\bar{Z}(z^\star) \in \mathbb{R}^{32\times 32}, \tag{26}$$

which is not a diagonal matrix, and thus determining whether it is Hurwitz is not straightforward. For that purpose, we provide a similarity matrix, i.e., $P \in \mathbb{R}^{32\times 32}$, such that PAP^{-1} is a block triangular matrix, and where each block diagonal matrix is in controllable form (allowing us to invoke the results from Section V). Consider then

$$P := \begin{bmatrix} P_z & P_\theta & P_x & P_\delta & P_y & P_\psi & P_\perp \end{bmatrix}^T \in \mathbb{R}^{24\times 24}, \tag{27}$$

where (below A is the Jacobian in (26), and $e_1, \cdots, e_{32}$ are the canonical basis vectors in $\mathbb{R}^{32}$)

$$\begin{aligned}
P_z &:= \begin{bmatrix} \nu & A\nu & A^2\nu \end{bmatrix}\big|_{\nu=\frac{d_2e_{31}-d_1e_{32}}{d_2-d_1}} \in \mathbb{R}^{32\times 3},\\
P_\theta &:= \begin{bmatrix} \nu & A\nu & A^2\nu \end{bmatrix}\big|_{\nu=\frac{e_{31}-e_{32}}{d_2-d_1}} \in \mathbb{R}^{32\times 3},\\
P_x &:= \begin{bmatrix} e_1 & Ae_1 & A^2e_1 & A^3e_1 & A^4e_1 \end{bmatrix} \in \mathbb{R}^{32\times 5},\\
P_\delta &:= \begin{bmatrix} \nu & A\nu & A^2\nu \end{bmatrix}\big|_{\nu=e_7-e_{10}} \in \mathbb{R}^{32\times 3},\\
P_y &:= \begin{bmatrix} e_2 & Ae_2 & A^2e_2 & A^3e_2 & A^4e_2 \end{bmatrix} \in \mathbb{R}^{32\times 5},\\
P_\psi &:= \begin{bmatrix} e_5 & Ae_5 & A^2e_5 & A^3e_5 & A^4e_5 \end{bmatrix} \in \mathbb{R}^{32\times 5},
\end{aligned}$$

and, finally, where $P_\perp := (f'(z^\star))^T \in \mathbb{R}^{32\times 8}$.

Remark 4: Recall the state decomposition in (1), and that $\dot{z} = Az$, for the linearized motion around the equilibrium. Then (for brevity, denote $p = (x, y, z)$ and $n = (\cdot, \psi, \theta)$)

$$\begin{bmatrix} P_x^T z \\ P_\delta^T z \\ P_y^T z \\ P_\psi^T z \end{bmatrix} = \begin{bmatrix} (x^{(0)}, x^{(1)}, x^{(2)}, x^{(3)}, x^{(4)}) \\ (\delta^{(0)}, \delta^{(1)}, \delta^{(2)})|_{\delta = e_1^T(p_1 - p_2)} \\ (y^{(0)}, y^{(1)}, y^{(2)}, y^{(3)}, y^{(4)}) \\ (\psi^{(0)}, \psi^{(1)}, \psi^{(2)}, \psi^{(3)}, \psi^{(4)}) \end{bmatrix},$$

and (the equalities below can only be verified under an appropriate coordinate transformation)

$$\begin{bmatrix} P_z^T z \\ P_\theta^T z \end{bmatrix} = \begin{bmatrix} (z^{(-1)}, z^{(0)}, z^{(1)}) \\ (\theta^{(-1)}, \theta^{(0)}, \theta^{(1)}) \end{bmatrix}.$$

That is, P_x is associated with the x linear motion of the bar (fifth order system) and P_δ is associated with the x linear motion between the UAVs (third order system); P_y is associated with the y linear motion of the bar (fifth order system) and P_ψ is associated with the y angular motion of bar (fifth order system). And finally, P_z is associated with the z linear motion of the bar (third order system) and P_θ is associated with the z angular motion of bar (third order system). (The sum of the integral errors is then associated with the z linear position of the bar, and the difference is associated with the z angular position of the bar.)

Given the state matrix A in (26) and the similarity matrix P in (27), it then follows that

$$PAP^{-1} = \begin{bmatrix} A_{z,\theta} \oplus A_{x,\delta} \oplus A_{y,\psi} & \star \\ 0_{8\times 24} & -\lambda I_{8\times 8} \end{bmatrix} \in \mathbb{R}^{32\times 32}, \tag{28}$$

where (28) is a block triangular matrix, with the first block as a block diagonal matrix with three blocks (note that the λ in (28) is that chosen in (24)). Thus $\text{eig}(A) = \{-\lambda\} \cup \text{eig}(A_{z,\theta}) \cup \text{eig}(A_{x,\delta}) \cup \text{eig}(A_{y,\psi})$, and, therefore, determining whether the Jacobian A in (26) is Hurwitz amounts to checking whether each of the three blocks in (28) is Hurwitz. Let us look at each of these matrices separately, corresponding to three decoupled motions: longitudinal, lateral and vertical.

Remark 5: In what follows, we assume $d_1 = -d_2 =: d$ (for some d) when presenting the results. The results without these assumptions are found in [**?**].

A. Longitudinal motion

Recall Remark 4, and note that P_x and P_δ is associated to $A_{x,\delta} \in \mathbb{R}^{8\times 8}$ in (28). As such, $A_{x,\delta}$ is associated with the longitudinal motion, namely the x motion of the bar, and the x motion difference between the two UAVs.

In what follows denote

$$F_x \equiv F_x^n(k_{p,x}^1, k_{p,x}^2, k_{d,x}^1, k_{d,x}^2, k_r^1, k_r^2) \in \mathbb{R}^3,$$

where F_x is some function of the gains shown above. Note then that $A_{x,\delta}$ has a specific structure, namely (below $\star$ denotes a vector in $\mathbb{R}^5$)

$$A_{x,\delta} = \begin{bmatrix} A_x & e_5 F_x^T \\ e_3 \star^T & A_\delta \end{bmatrix} \in \mathbb{R}^{(5+3)\times(5+3)} \tag{29}$$

Notice that $A_{x,\delta}$ can be rendered block triangular, if one chooses the gains such that F_x in (29) vanishes. That is accomplished if, for $i \in \{1, 2\}$, (below $(-1)^i = \pm 1$)

$$\begin{aligned} k_{p,x}^i &= k_{p,x} + (-1)^i \frac{gm}{4}\left(\frac{1}{l_1 m_1} - \frac{1}{l_2 m_2}\right) \\ k_{d,x}^i &= k_{d,x} + (-1)^i \frac{gm}{4k_r}\left(\frac{1}{l_1 m_1} - \frac{1}{l_2 m_2}\right) \\ k_r^1 &= k_r^2 = k_r, \end{aligned}$$

for some positive $k_{p,x}$, $k_{d,x}$, and k_r. That is, the proportional and derivative gains of each vehicle must be the same up to some difference that is proportional to the asymmetry of the system. If the vehicles' gains are chosen as above, then

$$A_{x,\delta} = \begin{bmatrix} A_x & 0_{5\times 3} \\ \star_{3\times 5} & A_\delta \end{bmatrix} \in \mathbb{R}^{8\times 8} \tag{31}$$

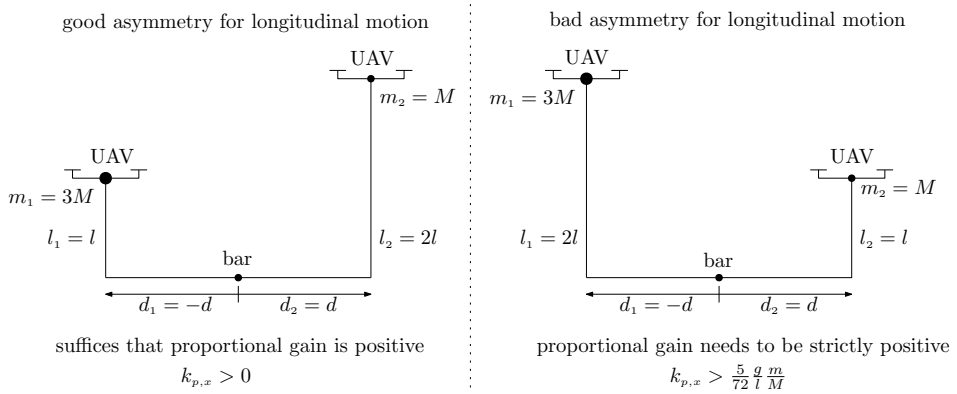

Fig. 4: Good and bad asymmetries (a good symmetry only requires the proportional gain to be positive, and a bad symmetry requires the proportional gain to be strictly positive): better for the heavier UAV to be attached to the shorter cable.

where (recall Γ_5 in (19))

$$A_x = \Gamma_5\left(p, f, k\right)|_{f_d=k_r, k=(k_{p,x}, k_{d,x})},$$
$$f_p = \frac{g(l_1+l_2)}{2l_1l_2}$$
$$p_1 = \frac{m(l_2-l_1)(l_1m_1-l_2m_2)}{2m_1m_2(l_1+l_2)^2}, p_2 = \frac{m(l_1^2m_1+l_2^2m_2)}{m_1m_2(l_1+l_2)^2},$$

and where (recall Γ_3 in (18))

$$A_\delta = \Gamma_3\left(f, k\right)|_{f_p=\frac{gm(l_1m_1+l_2m_2)}{4l_1m_1l_2m_2}, f_d=k_r, k=(k_{p,x}, k_{d,x})}.$$

It follows from (20) that A_x and A_δ are Hurwitz, provided that

$$k_{p,x} > \max(0, -f_p p_1) \text{ and } k_r > \frac{k_{p,x}}{k_{d,x}}.$$

i.e., provided that the proportional gain is big enough, and provided that the attitude gain is big enough. The latter constraint can be comprehended intuitively: fast tracking along the longitudinal direction requires a fast attitude inner loop.

Remark 6: If the system is symmetric (see (29)), then

$$A_x = \Gamma_5\left(p, f, k\right)|_{(p_1,p_2)=(0,\frac{m}{2M}),(f_p,f_d)=(\frac{g}{l},k_r),k=(k_{p,x},k_{d,x})}.$$

That is, the (linearized) x motion of the bar is exactly the motion of a container, with a cable of length l, being pulled by a crane of mass $2M$, and with a motor constant k_r.

Remark 7: As illustrated in Fig. 4, there are *good and bad* asymmetries; i.e, there are (good) asymmetries that only require $k_{p,x}$ to be positive, and there are (bad) asymmetries that require $k_{p,x}$ to be strictly positive. For the symmetric case (where (29) holds), it suffices for $k_{p,x}$ to be positive.

Remark 8: Recall Remark 4. It follows from (31) that, for the linearized motion, (denote $X := (x^{(0)}, \cdots, x^{(4)})$ and $\Delta := (\delta^{(0)}, \cdots, \delta^{(2)})$)

$$\begin{bmatrix}\dot{X}\\ \dot{\Delta}\end{bmatrix} = \begin{bmatrix}A_x & 0_{5\times 3}\\ \star_{3\times 5} & A_\delta\end{bmatrix}\begin{bmatrix}X\\ \Delta\end{bmatrix},$$

i.e., the x motion behaves as a fifth order integrator (similarly to (23)) decoupled from the δ motion; while the δ motion behaves as a third order integrator, cascaded after the x motion.

B. Lateral motion

Recall Remark 4, and note that P_y and P_ψ is associated to $A_{y,\psi} \in \mathbb{R}^{10\times 10}$ in (28). As such, $A_{\psi,\psi}$ is associated with the lateral motion, namely the y linear motion of the bar, and the y angular motion of the bar (yaw motion). In what follows denote

$$F_y \equiv F_y(k^1_{p,y}, k^2_{p,y}, k^1_{d,y}, k^2_{d,y}, k^1_{p,\psi}, k^2_{p,\psi}, k^1_{d,\psi}, k^2_{d,\psi}, k^1_r, k^2_r) \in \mathbb{R}^5,$$

where F_y is some function of the gains shown above. Note then that $A_{y,\psi}$ has a specific structure, namely

$$A_{y,\psi} = \begin{bmatrix}A_x & e_5F_y^T\\ e_5\tilde{F}_y^T & A_\theta\end{bmatrix} \in \mathbb{R}^{(5+5)\times(5+5)}. \tag{32}$$

Notice that $A_{y,\delta}$ can be rendered block triangular, if one chooses the gains such that either F_y or $\tilde{F}_y$ in (32) vanishes. We choose to cancel F_y, which is accomplished for some proper choice of gains, similarly to as in Subsection VI-A. Indeed, that is accomplished if, for $i \in \{1,2\}$, (below $(-1)^i = \pm 1$)

$$\begin{aligned} &k^i_{p,y} = k_{p,y} + (-1)^i \delta_y, k^i_{d,x} = k_{d,x} + (-1)^i \frac{\delta_y}{k_r} \\ &k^i_{p,\psi} = k_{p,\psi} + (-1)^i \delta_\psi, k^i_{d,\psi} = k_{d,\psi} + (-1)^i \frac{\delta_\psi}{k_r}. \\ &k^1_r = k^2_r = k_r, \end{aligned} \tag{33}$$

where

$$\begin{aligned} \delta_y &= \frac{gm}{2} \frac{2d^2(l_1-l_2)m_1m_2 + J(l_1m_1 - l_2m_2)}{2Jl_1l_2m_1m_2} \\ \delta_\psi &= \frac{4Jk_{p,y}(l_1-l_2)l_1l_2m_1m_2 - g(l_1+l_2)m(2d^2(l_1-l_2)m_1m_2 + J(l_1m_1 - l_2m_2))}{8Jl_1^2l_2^2m_1m_2}, \end{aligned}$$

and for some positive gains $k_{p,y}, k_{p,y}, k_{p,y}$ and $k_{d,\psi}$. That is, the proportional and derivative y-gains of each vehicle must be the same up to some difference that is proportional to the asymmetry of the system. If the vehicles' gains are chosen as in (33) with $k_{p,\psi} = \delta_\psi$ and $k_{d,\psi} = \frac{\delta_\psi}{k_r}$, then

$$\begin{aligned} A_y &= \Gamma_5(p,f,k)\,|_{p=\bar{p},f_p=\bar{f}_p,f_d=k_r,k=(k_{p,y},k_{d,y})}, \\ A_\psi &= \Gamma_5(p,f,k)\,|_{p=\tilde{p},f_p=\tilde{f}_p,f_d=k_r,k=(k_{p,y},k_{d,y})}, \end{aligned}$$

where

$$\begin{aligned} \bar{f}_p &= \frac{g(l_1+l_2)}{2l_1l_2}, \\ \bar{p}_1 &= -\frac{(l_1-l_2)m(2d^2(l_1-l_2)m_1m_2 + J(l_1m_1 - l_2m_2))}{2J(l_1+l_1)^2m_1m_2)}, \\ \bar{p}_2 &= m\frac{d^2(l_1-l_2)^2m_1m_2 + J(L_1^2m_1 + L_2^2m_2)}{J(l_1+l_2)^2m_1m_2} > 0, \\ \tilde{f}_p &= \frac{gmd^2}{Jl_1}, \\ \tilde{p}_1 &= \frac{2d^2(l_1-l_2)m_1m_2 + J(l_1m_1 - l_2m_2)}{4d^2L_2m_1m_2}, \\ \tilde{p}_2 &= \frac{J}{2d^2m_1}, \end{aligned}$$

and which are both Hurwitz, provided that

$$k_{p,y} > \max(0, -\bar{f}_p\bar{p}_1, -\tilde{f}_p\tilde{p}_1), k_r > \frac{k_{p,y}}{k_{d,y}}.$$

i.e., provided that the proportional gain is big enough, and provided that the attitude gain is big enough. Note that similar remarks to Remark 6, 7 and 8 can be made at this point regarding the lateral motion.

C. Vertical motion

Recall Remark 4, and note that P_z and P_θ is associated to $A_{z,\theta} \in \mathbb{R}^{6\times 6}$ in (28). As such, $A_{z,\theta}$ is associated with the vertical motion, namely the z linear motion of the bar, and the z angular motion of the bar (pitch motion).

In what follows denote

$$F_z \equiv F_z(k^1_{p,z}, k^2_{p,z}, k^1_{d,z}, k^2_{d,z}, k^1_{i,z}, k^2_{i,z},) \in \mathbb{R}^3,$$

where F_z is some function of the gains shown above. Note then that $A_{z,\theta}$ has a specific structure, namely

$$A_{z,\theta} = \begin{bmatrix} A_z & e_3F_z^T \\ e_3\tilde{F}_z^T & A_\delta \end{bmatrix} \in \mathbb{R}^{(3+3)\times(3+3)}. \tag{34}$$

Notice that $A_{z,\theta}$ can be rendered block triangular, if one chooses the gains such that either F_z or $\tilde{F}_z$ in (34) vanish. We choose to cancel F_z, implying that we decouple the z linear motion, from the z angular motion. That is accomplished if ($i \in \{1,2\}$)

$$\frac{k^1_{p,z}}{k^2_{p,z}} = \frac{k^1_{d,z}}{k^2_{d,z}} = \frac{k^1_{i,z}}{k^2_{i,z}} = \frac{m_1(J+2d^2m_2)}{m_2(J+2d^2m_1)}.$$

That is, the proportional, derivative and integral gains of each vehicle must respect a ratio, which is exactly 1 under symmetry conditions (see (**??**)). In order to satisfy the conditions above, let, for $h \in \{p, i, d\}$,

$$k^1_{h,z} = \frac{2(J + 2d^2 m_1)m_2}{4d^2 m_1 m_2 + J(m_1 + m_2)} k_{h,z},$$
$$k^2_{h,z} = \frac{2(J + 2d^2 m_2)m_1}{4d^2 m_1 m_2 + J(m_1 + m_2)} k_{h,z}, \tag{35}$$

for some positive $k_{p,z}$, $k_{d,z}$, and $k_{i,z}$. If the vehicles' gains are chosen as in (35), then

$$A_{z,\theta} = \begin{bmatrix} A_z & 0_{3\times 3} \\ \star_{3\times 3} & A_\theta \end{bmatrix} \in \mathbb{R}^{(3+3)\times(3+3)}$$

where (recall C_3 in (17))

$$A_z = C_3\left(\gamma_z(k^1_{p,z}, k^1_{d,z}, k^1_{i,z})\right)$$
$$A_\theta = C_3\left(\gamma_\theta(k^1_{p,z}, k^1_{d,z}, k^1_{i,z})\right)$$

where

$$\gamma_z = \frac{4m_1 m_2 (J + 2d^2 m_1)(J + 2d^2 m_2)}{(4d^2 m_1 m_2 + J(m_1 + m_2))(J(m + m_1 + m_2) + d^2(4m_1 m_2 + (m_1 + m_2)m))}$$
$$\gamma_\theta = \frac{4d^2 m_1 m_2}{4d^2 m_1 m_2 + J(m_1 + m_2)}$$

It follows from (17) that A_z and A_θ are Hurwitz (and therefore $A_{z,\theta}$), provided that

$$k_{i,z} < \min(\gamma_z, \gamma_\theta) k_{p,z} k_{d,z}.$$

i.e., provided that the integral gain is *small enough*. Note that, for a regular PID, it is required that $k_{i,z} < k_{p,z}k_{d,z}$, while the constraint above is more restrictive, since $\gamma_\theta < 1$. Moreover, notice that γ_θ is proportional to d (the distance of the contact points to the bar's center of mass): as such, it is advisable to have *big* a d (*big* compared with $\sqrt{\frac{J}{m_1+m_2}}$), because γ_θ is closer to 1 (and thus the bound on the integral gain is less restrictive). This also agrees with intuition, which suggests that controlling the bar's attitude when the contact points are too close to the bar's center of mass is difficult.

Remark 9: For the vertical motion (regarding its stability), the attitude gains of the vehicles do not play a role.

VII. Experimental Results

A video of the experiment that is described in the sequel is found at https://youtu.be/rgweowQ8fAE, whose results are visualized in Fig. 5. For the experiment, two hexacopters were used, namely one ASTEC-Neo weighting 2.22 kg, and one Tarot FY680 weighting 3.53 kg. The bar was made out of a core of aluminum, surrounded with PVC pipe, and with two metal plates at the contact points with the cables: in total, it weighted 1.48 kg, with the individual plates weighting 0.6 kg each (the bar's weight corresponds to 60% of the ASTEC-Neo and to 40% of the Tarot FY680). The bar has a length of 2m, with the contact points between the bar and the cables at the extremities of the bar, and thus $d_1 = -d_2 = 1$ m; the cables are attached to the bar's contact points by means of permanent magnets. The ASTEC-Neo is tethered to the bar by a 1.45 m cable, and the Tarot FY680 by a 1.2 m cable. The commands for controlling the hexacopter were processed on a ground station, developed in a ROS environment, and sent to the on-board autopilot, which allowed for remotely controlling the aerial vehicles. The ASTEC-Neo is equipped with a proprietary flight controller, which we communicate with by publishing a message of the type mav_msgs/RollPitchYawrateThrust; while the Tarot FY680 is equipped with an open source flight controller (namely a PixHawk), which we communicate with by publishing a message of the type mavros_msgs/OverrideRCIn. The hexacopter's and the bar's poses and twists were estimated by 12 cameras from a Qualisys motion capture system.

In the beginning of the experiment the bar is required to stabilize around $z^\star$ (see (10)) where $p^\star = (0.4, -0.5, 0.4)$m and $n^\star = e_2$ (see Remark 1), i.e, the bar is required to hover at 0.4m and required to be aligned with the y-axis. In Fig. 5(b), the bar attitude is parameterized with a pitch and yaw angle (i.e., $n = (\cos(\theta)\cos(\psi), \cos(\theta), \sin(\theta))$), and, as can be seen in Fig. 5(b) the bar is initially aligned with the y-axis ($\psi = 90°$). At around 55 sec, the bar is required to translate 0.5m in the x-direction, and at around 60 sec, the bar is required to align itself with the x-axis ($n^\star = e_1 :\Leftrightarrow \psi^\star = 0°$), which can be seen in Figs. 5(a) and 5(a). At around 80 sec, the bar is required to move in the y-direction, while keeping the same orientation, which can again be seen in Figs. 5(a) and 5(a). During the same experiment, we also tested robustness against impulse disturbances, which illustrate the size of the basin of attraction of the equilibrium. First, at around 100s, we disturbed the Tarot FY680 in the y-direction, as can be seen in Fig. 5(d); and, at around 110s, we disturbed the ASTEC-Neo in the y-direction, as can be seen in Fig. 5(c). In both cases, the system returns to its equilibrium point.

In Figs. 5(e) and 5(f), the control inputs are shown, and in Fig. 5(g) the integral terms for both UAVs are shown. The equilibrium integral term is inversely proportional to the vehicle's weight, which explains why the integral term for the

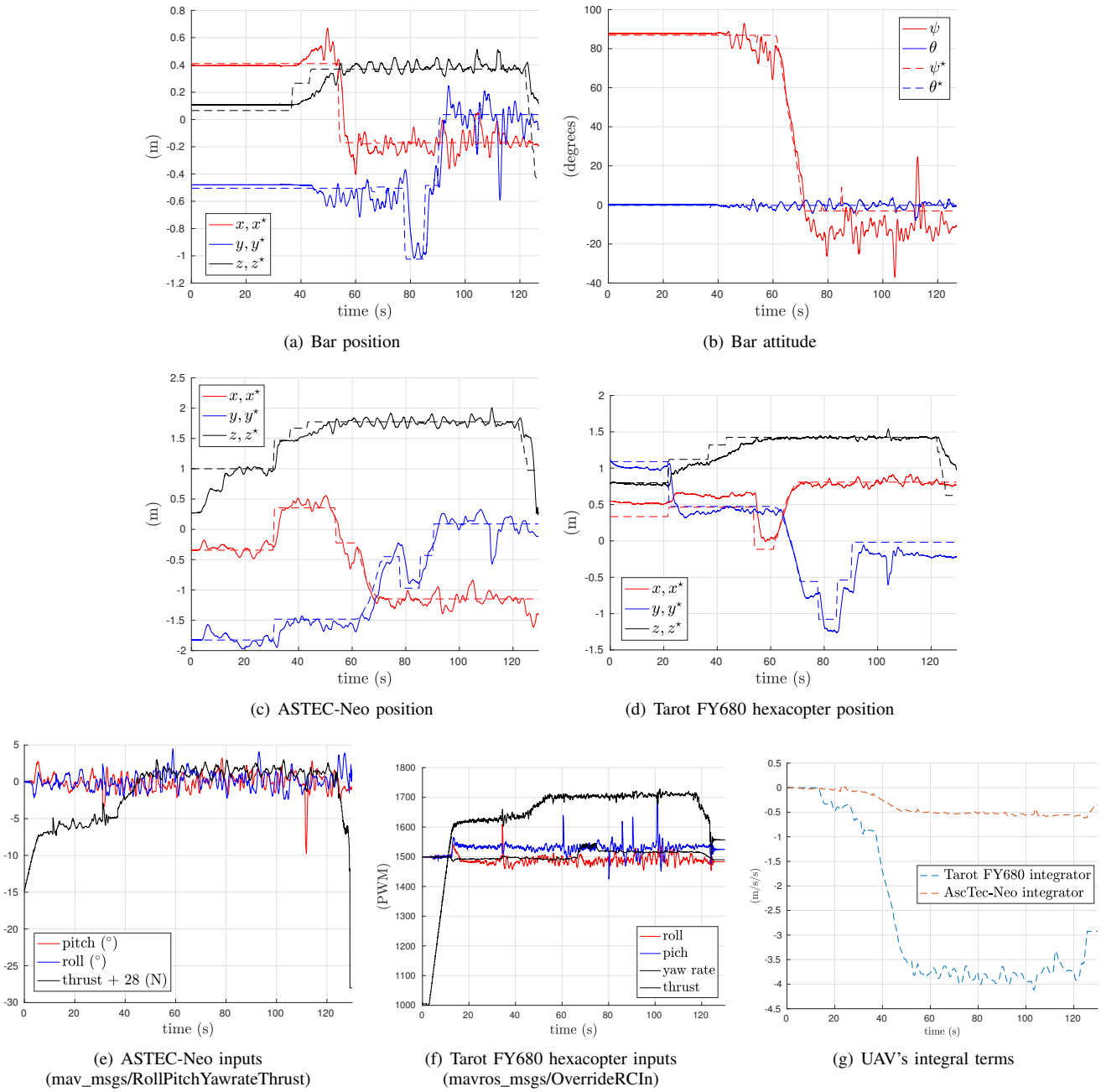

(a) Bar position

(b) Bar attitude

(c) ASTEC-Neo position

(d) Tarot FY680 hexacopter position

(e) ASTEC-Neo inputs (mav_msgs/RollPitchYawrateThrust)

(f) Tarot FY680 hexacopter inputs (mavros_msgs/OverrideRCIn)

(g) UAV's integral terms

Fig. 5: Experimental results for collaborative bar lifting.

ASTEC-Neo is smaller than that for the Tarot FY680.

References

[1] AEROWORKS aim. http://www.aeroworks2020.eu/.

[2] S. J. Lee and H. J. Kim. Autonomous swing-angle estimation for stable slung-load flight of multi-rotor uavs. In *2017 IEEE International Conference on Robotics and Automation (ICRA)*, pages 4576–4581, May 2017.

[3] P. O. Pereira and D. V. Dimarogonas. Stability of load lifting by a quadrotor under attitude control delay. In *2017 IEEE International Conference on Robotics and Automation (ICRA)*, pages 3287–3292, May 2017.

[4] M. Bisgaard, A. la Cour-Harbo, and J. D. Bendtsen. Adaptive control system for autonomous helicopter slung load operations. *Control Engineering Practice*, 18(7):800 – 811, 2010. Special Issue on Aerial Robotics.

[5] I. Palunko, R. Fierro, and P. Cruz. Trajectory generation for swing-free maneuvers of a quadrotor with suspended payload: A dynamic programming approach. In *2012 IEEE International Conference on Robotics and Automation*, pages 2691–2697, May 2012.

[6] S. Tang and V. Kumar. Mixed integer quadratic program trajectory generation for a quadrotor with a cable-suspended payload. In *2015 IEEE International Conference on Robotics and Automation (ICRA)*, pages 2216–2222, May 2015.

[7] M. Tognon and A. Franchi. Dynamics, control, and estimation for aerial robots tethered by cables or bars. *IEEE Transactions on Robotics*, 33(4):834–845, Aug 2017.

[8] J. Thomas, G. Loianno, K. Sreenath, and V. Kumar. Toward image based visual servoing for aerial grasping and perching. In *2014 IEEE International Conference on Robotics and Automation (ICRA)*, pages 2113–2118, May 2014.

[9] R. Mebarki, V. Lippiello, and B. Siciliano. Toward image-based visual servoing for cooperative aerial manipulation. In *2015 IEEE International Conference on Robotics and Automation (ICRA)*, pages 6074–6080, May 2015.

[10] S. Kim, S. Choi, H. Lee, and H. J. Kim. Vision-based collaborative lifting using quadrotor uavs. In *2014 14th International Conference on Control, Automation and Systems (ICCAS 2014)*, pages 1169–1174, Oct 2014.

[11] M. Gassner, T. Cieslewski, and D. Scaramuzza. Dynamic collaboration without communication: Vision-based cable-suspended load transport with two quadrotors. In *2017 IEEE International Conference on Robotics and Automation (ICRA)*, pages 5196–5202, May 2017.

[12] H. Lee, H. Kim, and H. J. Kim. Planning and control for collision-free cooperative aerial transportation. *IEEE Transactions on Automation Science and Engineering*, PP(99):1–13, 2017.

[13] H. Kim, H. Lee, S. Choi, Y. k. Noh, and H. J. Kim. Motion planning with movement primitives for cooperative aerial transportation in obstacle environment. In *2017 IEEE International Conference on Robotics and Automation (ICRA)*, pages 2328–2334, May 2017.

[14] T. Lee. Collision avoidance for quadrotor uavs transporting a payload via voronoi tessellation. In *2015 American Control Conference (ACC)*, pages 1842–1848, July 2015.

[15] Hyeonbeom Lee, Hyoin Kim, and H. J. Kim. Path planning and control of multiple aerial manipulators for a cooperative transportation. In *2015 IEEE/RSJ International Conference on Intelligent Robots and Systems (IROS)*, pages 2386–2391, Sept 2015.

[16] Q. Jiang and V. Kumar. The inverse kinematics of cooperative transport with multiple aerial robots. *IEEE Transactions on Robotics*, 29(1):136–145, Feb 2013.

[17] N. Michael, J. Fink, and V. Kumar. Cooperative manipulation and transportation with aerial robots. *Autonomous Robots*, 30(1):73–86, 2011.

[18] M. Mohammadi, A. Franchi, D. Barcelli, and D. Prattichizzo. Cooperative aerial tele-manipulation with haptic feedback. In *2016 IEEE/RSJ International Conference on Intelligent Robots and Systems (IROS)*, pages 5092–5098, Oct 2016.

[19] C. Masone, H. H. Bülthoff, and P. Stegagno. Cooperative transportation of a payload using quadrotors: A reconfigurable cable-driven parallel robot. In *2016 IEEE/RSJ International Conference on Intelligent Robots and Systems (IROS)*, pages 1623–1630, Oct 2016.

[20] Daniel Mellinger, Michael Shomin, and Vijay Kumar. Control of quadrotors for robust perching and landing. In *Proceedings of the International Powered Lift Conference*, pages 205–225, 2010.

[21] A. Gawel, M. Kamel, T. Novkovic, J. Widauer, D. Schindler, B. P. von Altishofen, R. Siegwart, and J. Nieto. Aerial picking and delivery of magnetic objects with mavs. In *2017 IEEE International Conference on Robotics and Automation (ICRA)*, pages 5746–5752, May 2017.

[22] A. Tagliabue, M. Kamel, S. Verling, R. Siegwart, and J. Nieto. Collaborative transportation using mavs via passive force control. In *2017 IEEE International Conference on Robotics and Automation (ICRA)*, pages 5766–5773, May 2017.

[23] P. Pereira and Dimos V. Dimarogonas. Collaborative transportation of a bar by two aerial vehicles with attitude inner loop and experimental validation. In *2017 Conference on Decision and Control*, 2017 (to appear).

[24] P. E. I. Pounds, D. R. Bersak, and A. M. Dollar. Grasping from the air: Hovering capture and load stability. In *2011 IEEE International Conference on Robotics and Automation*, pages 2491–2498, May 2011.

[25] M. Orsag, C. Korpela, M. Pekala, and P. Oh. Stability control in aerial manipulation. In *2013 American Control Conference*, pages 5581–5586, June 2013.

[26] J. Schultz and T. Murphey. Trajectory generation for underactuated control of a suspended mass. In *2012 IEEE International Conference on Robotics and Automation*, pages 123–129, May 2012.

[27] R. C. Nelson. *Flight stability and automatic control*, volume 2. WCB/McGraw Hill, 1998.